

**Iridium and rhodium analogues of the Shilov cycle catalyst;
and the investigation and applications of the
Reduction-Coupled Oxo Activation (ROA) mechanistic motif
towards alkane upgrading**

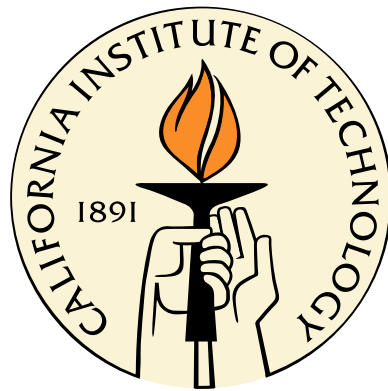
Thesis by

Ross Fu

In Partial Fulfillment of the Requirements

for the Degree of

Doctor of Philosophy



California Institute of Technology

Pasadena, California

2014

(Defended May 9th, 2014)

© 2014
Ross Fu
All Rights Reserved

To Annie, Bruce, Mom, Dad, and Harold.

Acknowledgments

There are many people who have helped me throughout the course of my graduate studies, and my education in general. Therefore, I cannot guarantee that this list will be comprehensive. First and foremost I want to thank my lovely wife, Annie Tigranyan, who through good times and bad has been a steady and ongoing source of support, encouragement, and motivation; and my parents, Prof. Xiang-Dong Fu and Dr. Mingjie Jin, who have shaped me to be the person I am and who have been the role models for the person I aspire to be. I also want to mention my son Bruce, who has been a continuing source of inspiration for me to be the best father I can; and Toshi, who has been my faithful and unwavering companion, guarding my side for many hours in the office as I put together this dissertation. Finally, I want to thank my parents and parents-in-law, Ruzanna Parvizi and Ashot Tigranyan, for their invaluable support in helping me raise my young family; and in particular my mother-in-law, who has devoted countless hours and effort taking care of Bruce so that I could concentrate on my work.

I am greatly indebted to my advisor, Prof. William Goddard, for accepting me into his research group despite my (at the time) purely experimental background, for his extensive help at the beginning of my computational training, and for his continuing mentorship and scientific insights. I also want to thank my previous advisor at Caltech, Prof. John Bercaw, for his mentorship in synthetic chemistry, for helping me initiate my graduate-level work in chemistry, and for his continued work on my thesis committee. In addition, I want to thank Prof. Theo Agapie for chairing my committee, and Prof. Thomas Miller for serving in my committee. Finally I also want to thank Dr. Jay Labinger and Prof. Robert Grubbs for serving in my previous committee during my candidacy exam.

In the Goddard group, *a.k.a.* the Materials Simulation Center, I want to especially thank the director for catalysis, Dr. Robert “Smith” Nielsen, for his collaboration, teaching, advice, patience, and incredible depth of knowledge. I also want to thank my various collaborators, including Prof. Brent Gunnoe, Dr. George Fortman, Dr. Matthew O'Reilly, and Michael Webster-Gardiner at the University of Virginia, and Prof. Greg Fu, Dr. Nathan Schley, and Trixia Buscagan at Caltech. In addition, I want to thank many other group members for their advice, discussions, and friendship; including but not limited to Dr. Mu-Jeng Cheng, Dr. Wei-Guang Liu, Dr. José Mendoza-Cortés, Dr. Julius Su, Samantha Johnson, Yanchoi Lam, Fan Liu, and Caitlin Scott.

In the Bercaw group, I want to thank Dr. Jay Labinger for his invaluable advice in the preparation of my *Organometallics* publication. I also want to thank the help and advice of my fellow students and postdocs Dr. Steve Baldwin, Dr. George Chen, Prof. Nilay Hazari, Dr. Rachel Klet, Dr. Valerie Kristof, Dr. Taylor Lenton, Prof. Alex Miller, Prof. Ian Tonks, Prof. Dave Weinberg, Prof. Nathan West, Dr. Matt Winston, Yanchoi Lam, Josef Meier, and Tonia Ahmed.

I also want to thank Larry Henling and Dr. Michael Day for help in X-ray crystallography, and Naseem Tourian and Dr. Mona Shahgholi for their help in mass spectrometry.

Finally, I want to thank the many friends who have made my years here at Pasadena so enjoyable. In particular, Elena Bibikova, Jerry Koo and Fiona Chiang, Tracey Liu, Hemanth Siriki, Jerzy Szablowski, Chloe Wang, Arlene Santos and the Salsa Club and of course my dance partner Annie Tigranyan; and some of my oldest friends from high school, Michael Liao, Jason Lin, Erik Tsou, and David Wang.

Abstract

This dissertation will cover several disparate topics, with the overarching theme centering on the investigation of organometallic C–H activation and hydrocarbon transformation and upgrading. Chapters 2 and 3 discuss iridium and rhodium analogues of the Shilov cycle catalyst for methane to methanol oxidation, and Chapter 4 on the recently discovered ROA mechanistic motif in catalysts for various alkane partial oxidation reactions. In addition, Chapter 5 discusses the mechanism of nickel pyridine bisoxazoline Negishi catalysts for asymmetric and stereoconvergent C–C coupling, and the appendices discuss smaller projects on rhodium H/D exchange catalysts and DFT method benchmarking.

Chapter 2: The iridium complex $(\text{ONO})\text{Ir}(\text{PPh}_3)_2\text{Me}$, where (ONO) is a bis(phenolate)pyridine pincer ligand, undergoes C–H activation of benzene, related arenes, and acetonitrile. Labeling and kinetic studies indicate a unique and heretofore undescribed mechanism involve intramolecular C–H activation followed by intermolecular C–H activation.

Chapter 3: The Shilov catalytic cycle for methane to methanol oxidation *via* a homogeneous Pt catalyst has long been a target of investigation, with work focusing on improving catalyst stability, yield, and robustness. A Rh analogue to the Shilov cycle was explored due to its increased stability at high oxidation states. A density functional theory-driven virtual screening of ligand frameworks revealed that the fluorine-substituted amidinate (NN^{F}) ligand provides the lowest transition state energies for methane C–H activation and methyl group functionalization, and stands most promising as a target for experimental investigation.

Chapter 4: The vanadium phosphorus oxide (VPO) catalyst has been used in industry for the remarkably selective conversion of butane to maleic anhydride. Investigation of the reaction mechanism revealed the surprising conclusion that, although redox action occurs in the vanadium centers as expected, initial C–H activation takes place in the phosphorus oxide moieties. Further work has revealed that the same phenomenon can be extended to other transition metal/nonmetal oxo pairs. This phenomenon, which has been named the Reduction-Coupled Oxo Activation (ROA) mechanistic motif, is attributed to the concomitant formation of a strong oxo-hydrogen bond on the nonmetal and a one-electron reduction on the transition

metal. Finally, a homogeneous vanadium phosphorus oxo complex is proposed to incorporate the novel ROA mechanistic pathway as a potential propane oxidation catalyst. Several oxidation pathways are proposed, leading to end products such as propylene, isopropanol, and propylene oxide. These assertions are supported with density functional theory calculations on the potential reaction pathways.

Chapter 5: The *in situ* generated Ni(*i*Pr–pybox) complex catalyzes enantioselectively the cross-coupling of secondary sp^3 -C substrates. This system is very notable for its property of stereoconvergence: *both* enantiomers of a racemic substrate may be converted into a single enantiomer of a product. This chapter will computationally explore the mechanism responsible for both the remarkable activity and selectivity of the Ni(*(S,S)*–*i*Pr–pybox system; such a mechanism is believed to deviate substantially from the canonical “textbook” mechanism of Negishi coupling. Furthermore, a generalized calculation scheme is presented that allows for the rapid enantioselectivity prediction of many related pybox ligands as well, in order to help predict the next generation of asymmetric Negishi coupling catalysts.

Contents

Acknowledgments	iv
Abstract	vi
1 Introduction	1
1.1 Iridium and Rhodium analogues of the Shilov cycle catalyst	1
1.2 Investigation and applications of the Reduction-Coupled Oxo Activation (ROA) mechanistic motif towards alkane upgrading.	3
1.3 Other projects	4
1.4 References	6
2 Intra- and intermolecular C–H bond activation by bis(phenolate)pyridineiridium(III) complexes	8
2.1 Abstract	8
2.2 Introduction	9
2.3 Results and Discussion	9
2.3.1 Synthesis and Characterization of Ir ^I complexes	9
2.3.2 Synthesis and Characterization of Ir ^{III} Complexes	13
2.3.3 C–H Activation by Ir ^{III} (ONO ^{tBu}) Complexes	21
2.3.4 Kinetics of C–H Activation	28
2.4 Conclusions	32
2.5 Supporting Details	32
2.5.1 Experimental Section	32
2.5.2 Kinetics Details	46
2.5.3 Crystallographic Data	46
2.6 Acknowledgments	46
2.7 References	53

3 DFT virtual screening identifies rhodium-amidinate complexes as active homogeneous catalysts for methane to methanol oxidation	56
3.1 Abstract	56
3.2 Introduction	57
3.3 Materials and Methods	58
3.4 Results	60
3.4.1 The Rh(NN) complexes in TFAH	63
3.4.2 The Rh(NN ^F) complexes in TFAH	67
3.4.3 The Rh(NN ^F) complexes in water	67
3.4.4 The Rh(ONN ^x) family of complexes in TFAH	73
3.4.5 The Rh(DPMS) and Rh(DPES) complexes in TFAH	78
3.4.6 The Rh(PN) complexes in TFAH	78
3.4.7 The Rh(bisq ^x) family of complexes in TFAH	81
3.4.8 Product protection and C–H activation	92
3.5 Discussion	100
3.6 Conclusions	105
3.7 Acknowledgments	106
3.8 References	107
4 The Reduction-Coupled Oxo Activation mechanistic motif for C–H bond activation and oxidation	110
4.1 Abstract	110
4.2 Introduction	111
4.2.1 The VPO catalyst for <i>n</i> -butane oxidation	111
4.2.2 The ROA mechanistic motif	112
4.2.3 Potential homogeneous catalysts utilizing the ROA principle	115
4.3 Materials and methods	116
4.4 Validation of ROA on small oxide clusters	118
4.5 Reactions of a homogeneous oxidation catalyst utilizing the ROA mechanistic motif	128
4.5.1 Nomenclature	128
4.5.2 The resting V ^V state	129
4.5.3 Propane activation transition states	132
4.5.4 Monohydrogenated V ^{IV} states	136
4.5.5 Catalytic cycle involving H-atom abstraction only	136
4.5.6 Reduced V ^{III} states	139
4.5.7 Catalytic cycle involving H-atom abstraction followed by isopropyl addition .	143

4.5.8	Comparison of the catalytic cycles	144
4.6	Conclusions	146
4.7	References	147
5	The mechanism of Ni(<i>i</i>Pr–pybox) complexes as asymmetric Negishi C–C coupling catalysts	150
5.1	Abstract	150
5.2	Introduction	151
5.2.1	The Ni(<i>i</i> Pr–pybox) system	152
5.2.2	Existing computational work	154
5.3	Materials and methods	156
5.4	Results	157
5.4.1	The overall general mechanism	157
5.4.2	Nature of the organozinc reagent	158
5.4.3	Mechanism for Ni ^I oxidation and methylation	161
5.4.4	Mechanism for reductive elimination	166
5.5	Discussion	167
5.5.1	Overall catalytic cycle	167
5.5.2	Predictions for new ligands	167
5.6	Conclusions	171
5.7	Supporting figures	172
5.8	References	178
A	C–H activation using Rh^I complexes supported by bis-nitrogen chelating ligands	180
A.1	Abstract	180
A.2	Introduction	181
A.3	Materials and methods	181
A.4	Results and discussion	181
A.4.1	Experimental results	181
A.4.2	Computational results	184
A.5	Conclusions	187
A.6	References	188
B	Energy levels of group 10 transition metal atoms and ions	189
B.1	Abstract	189
B.2	Introduction	190
B.3	The neutral atom	190

B.3.1	Platinum (0)	191
B.3.2	Palladium (0)	193
B.3.3	Nickel (0)	194
B.4	The singly-charged cation	195
B.5	Angular momentum-dependent artifacts in DFT calculations	196
B.5.1	Angular momentum of the electron/hole in the d^1/d^9 configuration of the cation	196
B.5.2	Angular momentum of the holes in the d^8 configuration of the dication	199
B.6	Energies of d^2 and d^8 triplet states	199
B.6.1	Background	201
B.6.2	The d^2 and d^8 triplet states	202
B.6.3	Pure and mixed complex orbital configurations	204
B.6.4	Real orbital configuration energies	205
B.6.5	Summary	206
B.7	Conclusions	206
B.8	References	208

List of Figures

1.1	C–H activation by a phosphorus oxo leads to a one electron reduction on the neighboring vanadium.	4
2.1	The ONO and $\text{ONO}^{t\text{Bu}}$ ligands.	10
2.2	Crystal structure of pyridine-activated complex 2-3	11
2.3	Crystal structure of $[\text{NaIr}(\text{cod})(\text{ONO}^{t\text{Bu}})]_2$, 2-4	13
2.4	Crystal structure of $[\text{Ir}(\text{cod})]_2(\text{ONO}^{t\text{Bu}})$, 2-5	14
2.5	Crystal structure of $[(\text{ONO}^{t\text{Bu}})\text{Ir}(\text{cod})(\text{MeCN})]\text{[PF}_6]$, 2-6	14
2.6	Crystal structure of $[(\text{ONO}^{t\text{Bu}})\text{Ir}(\text{cod})\text{OTf}$, 2-7	15
2.7	Crystal structure of <i>trans</i> -($\text{ONO}^{t\text{Bu}}$) $\text{Ir}(\text{PPh}_3)_2\text{OTf}$, 2-8	16
2.8	Crystal structure of <i>trans</i> -($\text{ONO}^{t\text{Bu}}$) $\text{Ir}(\text{PPh}_3)_2\text{OH}$, 2-9	17
2.9	Crystal structure of ($\text{ONO}^{t\text{Bu}}$) $\text{Ir}(\text{PPh}_3)_2\text{H}$, 2-11	17
2.10	Crystal structure of ($\text{ONO}^{t\text{Bu}}$) $\text{Ir}(\text{PPh}_3)_2\text{Me}$, 2-12	19
2.11	Crystal structure of ($\text{ONO}^{t\text{Bu}}$) $\text{Ir}(\text{PPh}_3)_2\text{I}$, 2-13	19
2.12	Crystal structure of ($\text{ONO}^{t\text{Bu}}$) $\text{Ir}(\text{PEt}_3)_2\text{Me}$, 2-14	20
2.13	Crystal structure of ($\text{ONO}^{t\text{Bu}}$) $\text{Ir}(\text{PEt}_3)_2\text{I}$, 2-15	21
2.14	Cyclic voltammetry of 2-14	22
2.15	EPR spectrum of $[(\text{ONO}^{t\text{Bu}})\text{Ir}(\text{PEt}_3)_2\text{Me}]\text{PF}_6$, 2-16	22
2.16	Crystal structure of $[(\text{ONO}^{t\text{Bu}})\text{Ir}(\text{PEt}_3)_2\text{Me}]\text{PF}_6$, 2-16	23
2.17	Crystal structure of ($\text{ONO}^{t\text{Bu}}$) $\text{Ir}(\text{PPh}_3)_2\text{Ph}$, 2-17	24
2.18	Crystal structure of ($\text{ONO}^{t\text{Bu}}$) $\text{Ir}(\text{PPh}_3)[\kappa^2\text{-PPh}_2(o\text{-C}_6\text{H}_4)]$, 2-18	24
2.19	Crystal structure of $[(\text{ONO}^{t\text{Bu}})\text{Ir}(\text{PPh}_3)(\mu\text{-CH}_2\text{CN})]_2$, 2-19	26
2.20	Kinetics of conversion of 2-12 to 2-17 and their deuterated isotopologues.	30
2.21	Dependence of the reciprocal of the rate of conversion of 2-12 to 2-17 on the amount of added triphenylphosphine.	30
2.22	Kinetics for conversion of 2-17 to 2-18 in C_6D_6 and <i>p</i> -xylene- d_{10}	31
2.23	Conversion of 2-12 to 2-17-<i>d</i>₆ in C_6D_6 with varying amounts of extra PPh_3 added.	47
3.1	The rhodium-ligand complexes screened.	63

3.2	Rh(NN) transition state structures.	66
3.3	Rh(NN ^F) transition state structures.	69
3.4	Rh(NN ^F) in water transition state structures.	72
3.5	The various Rh ^{III} (bisq ^x)(Me) III-I S _N 2 functionalization transition states.	87
3.6	The various Rh ^{III} (bisq ^x)(Me) III-II S _R 2 functionalization transition states.	88
3.7	Graph of the activation and functionalization transition state energies of the various Rh(bisq ^x) complexes at 298 K and 498 K.	91
3.8	Transition states for the functionalization of methane, Me-TFA, and methanol using Rh(NN) complexes in TFAH.	93
3.9	Transition states for the functionalization of methane, Me-TFA, and methanol using Rh(NN ^F) complexes in TFAH.	94
3.10	Summary of the data presented in Figures 3.8, 3.9, and 3.11.	95
3.11	Comparison of activation energies for methane and for methanol in the same structure for Rh(NN ^F) complexes in water.	96
3.12	Comparison of the activation states of methane and methyl trifluoroacetate by Rh-(DPMS) complexes, showing the product protection afforded.	97
3.13	Comparison of the activation states of methane and methyl trifluoroacetate by Rh(DPES) complexes, showing the product protection afforded.	98
3.14	Comparison of the activation states of methane and methyl trifluoroacetate by the Rh(bisq ^x) family of complexes, showing the product protection afforded.	99
3.15	Graph of the methane activation energy of the various rhodium complexes <i>vs.</i> the 4s orbital energy of the rhodium in their resting states.	101
3.16	Graph of the methane activation energy of the various rhodium complexes <i>vs.</i> the Rh-C bond energy of the lowest-energy Rh-Me complex.	103
3.17	A graph of the Rh-TFA to Rh-Me change in the 4s orbital energy, a measure of the Rh atom's softness, versus the adjusted TS barrier.	104
3.18	The calculated free energy of the (NNC)Ir(TFA) ₂ system, <i>via</i> the same internal substitution mechanism applied to Rh ^{III} complexes.	105
4.1	O-H bond strength for oxygen atoms on the (V ^{IV} O) ₂ (P ₂ O ₇) surface.	111
4.2	Oxygen adsorption energies on the (V ^{IV} O) ₂ (P ₂ O ₇) surface and the O-H bond strength (D_H) to each of these O atoms.	112
4.3	O-H bond strengths for the various oxygen atoms on the X1-V ^V OPO ₄ surface.	113
4.4	C-H activation by a phosphorus oxo leads to a one electron reduction on the neighboring vanadium.	113

4.5	Use of finite cluster models to investigate how the O–H bond strength of P=O moieties varies based on the number of V coupled to it <i>via</i> O linkages.	114
4.6	Known complexes featuring a phosphinite ligand bound κ –P to a transition metal, and a proposed vanadium κ –P phosphinite complex.	116
4.7	General models for small oxide clusters.	118
4.8	Optimized structures of the $P_xV_{4-x}O_{10}$ species ($x \in \{0, 1, 2, 3\}$) and their monohydrogenated equivalents.	119
4.9	Optimized structures of the dihydrogenated $P_2V_2O_{10}H_2$ and trihydrogenated $P_2V_2O_{10}H_3$ species.	120
4.10	Optimized structures of the XV_3O_{10} species ($X \in \{P, As, Sb, Bi\}$) and their monohydrogenated $XV_3O_{10}H$ counterparts.	121
4.11	Optimized structures of the $Z_2V_2O_{11}$ species ($Z \in \{S, Se, Te\}$) and their monohydrogenated $Z_2V_2O_{11}H$ counterparts.	122
4.12	Optimized structures of the hydrated species $Te_2V_2O_{12}H_2$ and $Te_2V_2O_{12}H_3$	122
4.13	Optimized structures of the fully hydrated species $Te_2V_2O_{14}H_6$ and $Te_2V_2O_{14}H_7$	123
4.14	Optimized structures of $Se_2V_2O_9$ and $Te_2V_2O_9$, as well as their monohydrogenated counterparts $Se_2V_2O_9H$ and $Te_2V_2O_9H$	124
4.15	Optimized structures of the group 14-vanadium oxide species $Z_2V_2O_{10}H_2$, where $Z \in \{Si, Ge, Sn, Pb\}$; as well as that of their corresponding monohydrogenated species.	126
4.16	Optimized structures of the molybdenum-containing species $P_2Mo_2O_{11}$, $Te_2Mo_2O_{10}$, and $Te_2Mo_2O_{12}$; as well as that of their corresponding monohydrogenated species.	127
4.17	Template for the nomenclature of investigated (OPO)V complexes.	129
4.18	The geometry-optimized structures of $(OPO)_H^fV^V O^c(OH)^s(H_2O)^t$, $(OPO)^fV^V O^c(H_2O)_2^{st}$, and $[(OPO)^fV^V O^c(OH)_2^{st}]^{2-}$	133
4.19	The geometry-optimized structure of $[(OPO)_{H_iPr}^fV^V O^c(H_2O)_2^{st}]^\ddagger$	135
4.20	The geometry-optimized structures of $(OPO)_H^fV^{IV} O^c(H_2O)_2^{st}$, $(OPO)^fV^{IV} (OH)^c(H_2O)_2^{st}$, and $[(OPO)^fV^{IV} O^s(H_2O)_2^{ct}]^-$	136
4.21	The geometry-optimized structures of ${}^3(OPO)^fV^{III}(HOiPr)^s(H_2O)_2^{ct}$, ${}^3(OPO)^fV^{III}(H_2O)_3^{cst}$, and ${}^3(OPO)_H^fV^{III}(OH)^s(H_2O)^a$	144
5.1	The computationally studied reaction of the Ni(<i>i</i> Pr–pybox) Negishi coupling catalyst as reported by Lin et al.	155
5.2	The various $(MeZnI)_m(dma)_n$ species, where $m, n \in \{0, 1, 2\}$	159
5.3	The various $(ZnBrI)_m(dma)_n$ species, where $m, n \in \{0, 1, 2\}$	160
5.4	Transition states for the reductive elimination of 1-methylindane from various Ni^{III} – $((S, S)-iPr-pybox)(Me)ind$ species.	168

5.5	Reaction coordinate diagram of the entire catalytic cycle for the coupling of ind–Br and MeZnI to form ind–Me.	169
5.6	Modified ligands which may allow for different enantioselective properties as compared to the original (<i>i</i> Pr–pybox) ligand.	170
A.1	Temperature dependence <i>vs.</i> turnover numbers for complexes 1 and 2	182
A.2	Concentration of Rh dependence <i>vs.</i> TON for complexes 1 and 2	183

List of Schemes

1.1	The original Pt ^{II} /Pt ^{IV} cycle of the Shilov catalyst, as well as Ir ^{III} /Ir ^V and Rh ^I /Rh ^{III} analogues.	2
1.2	The oxidation of <i>n</i> -butane to maleic anhydride using vanadium phosphorus oxide as a catalyst.	3
1.3	The generalized mechanism of the Ni((<i>i</i> Pr)-pybox) Negishi coupling catalyst as it proceeds through a Ni ^I -Ni ^{III} cycle.	5
2.1	Synthesis of Na[Ir(cod)(ONO)], 2-1.	10
2.2	Synthesis of the ligand H ₂ (ONO ^{tBu}).	12
2.3	Synthesis and reactivity of [NaIr(cod)(ONO ^{tBu})] ₂ , 2-4.	12
2.4	Oxidation of [NaIr(cod)(ONO ^{tBu})] ₂ , 2-4, to Ir ^{III} species.	13
2.5	Synthetic routes to (ONO ^{tBu})Ir(PPh ₃) ₂ H, 2-11.	18
2.6	Methylation to (ONO ^{tBu})Ir(PPh ₃) ₂ Me, 2-12, and subsequent functionalization with I ₂ to (ONO ^{tBu})Ir(PPh ₃) ₂ I, 2-13.	18
2.7	Synthesis of (ONO ^{tBu})Ir(PEt ₃) ₂ complexes.	20
2.8	Proposed mechanism for the transformation of 2-12 in benzene to the kinetic product (ONO ^{tBu})Ir(PPh ₃) ₂ Ph, 2-17 and the thermodynamic product (ONO ^{tBu})Ir(PPh ₃)-[κ ² -PPh ₂ (<i>o</i> -C ₆ H ₄)], 2-18.	27
2.9	Simplified version of Scheme 2.8, used for kinetic analysis.	29
3.1	Hypothetical catalytic cycle for the activation and functionalization of methane. . .	62
3.2	Catalytic cycle for the activation and functionalization of methane using Rh(NN) complexes in TFAH.	64
3.3	Catalytic cycle for the activation and functionalization of methane using Rh(NN ^F) complexes in TFAH.	68
3.4	Catalytic cycle for the activation and functionalization of methane using Rh(NN ^F) complexes in water.	70
3.5	Transition states for the activation of methane using Rh(NN ^F) complexes in water. .	71

3.6	Transition states for the III-I functionalization pathway using Rh(NN ^F) complexes in water.	73
3.7	Transition states for the III-II functionalization pathway using Rh(NN ^F) complexes in water.	74
3.8	Transition states for the III-IV-II functionalization pathway using Rh(NN ^F) complexes in water.	74
3.9	Catalytic cycle for the activation and functionalization of methane using Rh(ONN) complexes in TFAH.	75
3.10	Catalytic cycle for the activation and functionalization of methane using Rh(ONN ^F) complexes in TFAH.	76
3.11	Catalytic cycle for the activation and functionalization of methane using Rh(ONN ^{NMe₂}) complexes in TFAH.	77
3.12	Catalytic cycle for the activation and functionalization of methane using Rh(DPMS) complexes in TFAH, <i>via</i> the Rh(III-I), Rh(III-II), and Rh(III-IV-II) pathways.	79
3.13	Catalytic cycle for the activation and functionalization of methane using Rh(DPES) complexes in TFAH, <i>via</i> the Rh(III-I), Rh(III-II), and Rh(III-IV-II) pathways.	80
3.14	Catalytic cycle for the activation and functionalization of methane using Rh(DPMS) complexes in TFAH, <i>via</i> the Rh(I-III) pathway.	81
3.15	Catalytic cycle for the activation and functionalization of methane using Rh(PN) complexes in TFAH, <i>via</i> the Rh(III-I) and Rh(III-II) pathways.	82
3.16	Catalytic cycle for the activation and functionalization of methane using Rh(PN) complexes in TFAH, <i>via</i> the Rh(I-III) pathway.	83
3.17	The inorganic Rh ^{III} (bisq ^x)(TFA) ₃ species and its protonated analogues [Rh ^{III} (bisq ^x)-(TFA) ₂ (TFAH)] ⁺ and [Rh ^{III} (bisq ^x)(TFA) ₂] ⁺	84
3.18	The various methane activation transition states [Rh ^{III} (bisq ^x)(TFA)(Me··H··TFA)] ^{±‡}	85
3.19	Comparison of the functionalization of Rh ^{III} (bisq ^x)(Me _{ax})(TFA) ₂ <i>via</i> the III-I S _N 2 and III-II S _R 2 pathways and the completion of the catalytic cycle.	89
3.20	Catalytic cycle for the activation and functionalization of methane using Rh(bisq ^x) complexes in TFAH, <i>via</i> the Rh(I-III) pathway.	90
3.21	A schematic diagram showing the metal activation of an R–H bond, for example, methane.	100
4.1	The oxidation of <i>n</i> -butane to maleic anhydride using vanadium phosphorus oxide as a catalyst.	111
4.2	Potential catalytic cycle involving H-atom abstraction only.	138
4.3	Potential catalytic cycle assuming isopropyl addition and V ^{III} formation.	145

5.1	The generalized cross-coupling reaction and its mechanism.	151
5.2	The general reaction of the Ni(<i>i</i> Pr–pybox) Negishi coupling catalyst.	152
5.3	The generalized mechanism of the Ni(<i>i</i> Pr–pybox) Negishi coupling catalyst as it proceeds through a Ni ^I -Ni ^{III} cycle.	158
5.4	Complexation of the various MeZnX and ZnX ₂ species with X [–] , where X ∈ {Br, I}.	159
5.5	Three potential pathways for the methylation and oxidation of Ni ^I ((<i>S, S</i>)– <i>i</i> Pr–pybox)Br to Ni ^{III} ((<i>S, S</i>)– <i>i</i> Pr–pybox)(Me)(ind)Br.	162
5.6	The dissociative pathway for the methylation of Ni ^I ((<i>S, S</i>)– <i>i</i> Pr–pybox)Br to Ni ^I –((<i>S, S</i>)– <i>i</i> Pr–pybox)Me.	162
5.7	Ni ^I ((<i>S, S</i>)– <i>i</i> Pr–pybox)Br by ind–Br to Ni ^{II} ((<i>S, S</i>)– <i>i</i> Pr–pybox)Br ₂ and ind.	163
5.8	Ni ^{II} ((<i>S, S</i>)– <i>i</i> Pr–pybox)Br ₂ and its subsequent methylation or recombination with ind· as part of the Ni ^{II} or Ni ^{III} pathways.	165
5.9	The methylation of Ni ^{III} ((<i>S, S</i>)– <i>i</i> Pr–pybox)Br ₂ ((<i>S</i>)–ind) to produce Ni ^{III} ((<i>S, S</i>)– <i>i</i> Pr–pybox)(Br)(ind)Me.	166
5.10	A generalized catalytic mechanism that Ni(R–pybox) complexes undergo in Negishi coupling.	170
5.11	Expanded diagram of Ni ^{II} ((<i>S, S</i>)– <i>i</i> Pr–pybox)Br ₂ methylation as part of the Ni ^{II} pathway.	173
5.12	Expanded diagram of Ni ^{III} ((<i>S, S</i>)– <i>i</i> Pr–pybox)Br ₂ ((<i>S</i>)–ind) methylation as part of the Ni ^{III} pathway.	174
5.13	The reactions of the various Ni ^{III} ((<i>S, S</i>)– <i>i</i> Pr–pybox)(Me)ind species that lead to the reductive elimination of ind–Me.	175
A.1	Synthesis of rhodium H/D exchange catalysts (DAB ^F)Rh(COE)(TFA) A-1 and (BOZO)-Rh(COE)(TFA) A-2.	182
A.2	Oxidative addition of benzene by Rh(DAB ^F) and Rh(BOZO) complexes A-3 and A-4.	184
A.3	Various possible pathways for the H/D exchange of benzene catalyzed by a Rh(DAB ^F) complex.	185
A.4	Various possible pathways for the H/D exchange of benzene catalyzed by a Rh(BOZO) complex.	186
A.5	Various possible pathways for the H/D exchange of methane catalyzed by a Rh(DAB ^F) complex.	187

List of Tables

2.1	Summary of the results of Figure 2.23, used to create Figure 2.21.	46
2.2	Crystallographic data for the complexes 2-4, 2-5, 2-6, and 2-7.	48
2.3	Crystallographic data for the complexes 2-8, 2-9, 2-10, and 2-11.	49
2.4	Crystallographic data for the complexes 2-12, 2-13, 2-14, and 2-15.	50
2.5	Crystallographic data for the complexes 2-16, 2-17, 2-18, and 2-19.	51
2.6	Crystallographic data for the complex $(ONO^{tBu})Ir(PEt_3)_2Cl$	52
3.1	Antoine equation parameters for trifluoroacetic acid and water.	60
3.2	Lowest activation and functionalization energies for each series of Rh-ligand complexes in TFAH.	65
3.3	Comparison of the various Rh parameters with the rhodium-ligands complexes' associated transition state barriers.	102
4.1	Comprehensive compilation of all $(OPO)V^V$ species studied.	132
4.2	Comprehensive compilation of all the transition states for propane activation by $(OPO)V^V$	135
4.3	Comprehensive compilation of all $(OPO)V^{IV}$ species studied.	137
4.4	Comprehensive compilation of all $(OPO)V^{IV}$ species studied.	142
4.5	Comprehensive compilation of all $(OPO)V^{IV}$ species studied.	143
5.1	Examples of various C–C cross-coupling reactions.	152
5.2	Some examples of substrates coupled by the $Ni(iPr\text{--pybox})$ catalyst.	153
5.3	Comparison of activation energies for various $Ni(R\text{--pybox})$ catalysts.	171
5.4	Relative energies of the neutral A , D , and G species for various $Ni(R\text{--pybox})$ complexes.	176
5.5	Relative energies of the cationic B , E , and H species for various $Ni(R\text{--pybox})$ complexes.	176
5.6	Relative energies of the cationic C , F , and J species for various $Ni(R\text{--pybox})$ complexes.	177
B.1	Relativistic <i>vs.</i> nonrelativistic Hartree-Fock excitation energies	190
B.2	Relativistic <i>vs.</i> nonrelativistic Hartree-Fock excitation energies for the M^+ ions.	191
B.3	Excitation energies of Pt atom as calculated by various DFTs.	191

B.4	Excitation energies of Pt atom calculated without <i>f</i> functions.	192
B.5	Excitation energies of Pt atom calculated using electron-correlation methods.	193
B.6	$d^{10} - d^9 s^1$ Excitation energies of Pd atom as calculated by Jaguar.	194
B.7	Excitation energies of Pd atom as calculated by Q-Chem.	194
B.8	Excitation energies of Ni atom as calculated by Q-Chem; electron-correlation methods. .	194
B.9	Excitation energies of Ni atom as calculated by Q-Chem; DFT methods.	195
B.10	Excitation energies of the group 10 atoms from d^9 to $d^8 s^1$, as calculated using various DFTs.	195
B.11	Excitation energies of the group 10 atoms from d^9 to $d^8 s^1$, as calculated using various electron-correlation methods.	196
B.12	“Degenerate” energies of the $\text{Pt}^+ d^9$ ground state.	197
B.13	“Degenerate” energies of the $\text{Pt}^{9+} d^1$ ground state.	197
B.14	“Degenerate” energies of the $\text{Ni}^+ d^9$ ground state as calculated by DFT methods. .	198
B.15	Degenerate energies of the $\text{Ni}^+ d^9$ ground state as calculated by electron-correlation methods.	198
B.16	Energies of the $\text{Pt}^{2+} d^8$ configuration, calculated by B3LYP/LACV3P**++.	199
B.17	Energies of the $\text{Pd}^{2+} d^8$ configuration, calculated by B3LYP/LACVP.	200
B.18	Energies of the $\text{Ni}^{2+} d^8$ configuration, calculated on Jaguar using the 6-31G(tm)**++ basis.	200
B.19	Energies of the $\text{Ni}^{2+} d^8$ configuration, experimental and calculated on Q-Chem using the G3LARGE basis.	201

Chapter 1

Introduction

1.1 Iridium and Rhodium analogues of the Shilov cycle catalyst

The facile, selective, and direct conversion of methane into methanol has long been a goal of industrial chemists [1]. Methane, the chief component of natural gas, is typically found in abundant quantities wherever petroleum deposits are found. However, due to its difficulty in liquefaction (its boiling point being only 110 K) and its relative paucity of demand as compared to other hydrocarbons, it is often not economical to harvest this gas, which is essentially a byproduct or co-product of petroleum recovery, and to transport it to market. Since methane is also a potent greenhouse gas, with a global warming potential 72 times more powerful than that of carbon dioxide [2], it cannot simply be released either. Hence it is often flared, a process that is both intrinsically wasteful and which results in a large amount of heat pollution.

One potential solution is to convert these vast quantities of methane into methanol. As methanol is liquid at room temperature and pressure, it is much more easily transported and stored. Methanol can be used as a fuel in flex fuel vehicles, blended with gasoline, or converted to gasoline or diesel fuel. In addition, it has many applications as an industrial solvent and chemical feedstock. As methanol is both more easily processed and in greater demand than methane, the efficient conversion from the former to the latter has the potential to be both environmentally friendly and economically favorable.

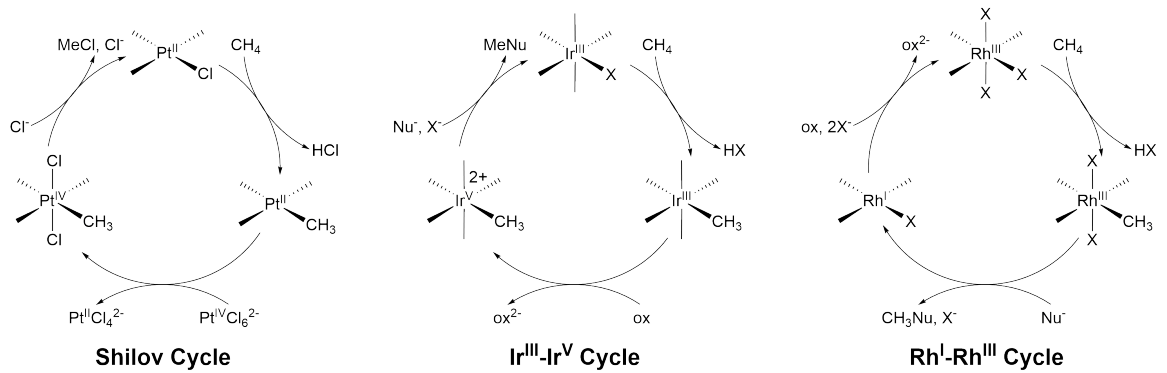
Although the reaction $\text{CH}_4 + \frac{1}{2}\text{O}_2 \longrightarrow \text{CH}_3\text{OH}$ is exoenergetic by 30 kcal/mol, efficient catalysis is hampered by the fact that the C–H bond dissociation energy (BDE) of methane is 104 kcal/mol, whereas the C–H BDE of methanol is only 95 kcal/mol. Hence, overoxidation is a major problem. In fact, potential methods that involve radicals have a theoretical maximum yield of only 5%, even with perfect conversion [3]. Hence, the currently favored industry-scale conversion of methane to methanol involves an indirect pathway *via* syngas [1]:



However, this pathway suffers from a difficult first step that is highly endergonic, requiring very high temperatures and pressures (700-1100°C, 40 atm). Hence, this state-of-the-art pathway requires large inputs of energy and very expensive production facilities despite the significantly exothermic nature of the overall reaction. An alternative mechanism that does not require such extreme conditions would thus be highly desirable.

Molecular compounds in solution have long been investigated as potential catalysts for this transformation, as they are typically well-defined, easy to characterize and model, and operate under relatively mild conditions. Much of the focus has been on routes involving C–H activation at a transition metal center followed by oxidative cleavage of the resulting C–M bond, which offer greater possibilities for good selectivity by avoiding radical-based pathways. Platinum complexes have received a great deal of attention [4], starting with Shilov's seminal work on the $\text{PtCl}_4^{2-}/\text{PtCl}_6^{2-}$ system, which can oxidize methane to methanol with some selectivity [5], and including the platinum bipyrimidine system, which has achieved the most impressive performance to date, converting methane to methyl bisulfate in up to 70% yield [6].

However, none of this platinum-based chemistry has yet been shown to lead to a practical process, owing in part to low reactivity, and a good deal of research activity has turned to other metals. Chapters 2 and 3 will address certain Ir and Rh analogues, respectively. The original Pt Shilov cycle, as well as modifications incorporating Ir and Rh, is given in Scheme 1.1.



Scheme 1.1. Left: The original $\text{Pt}^{\text{II}}/\text{Pt}^{\text{IV}}$ cycle of the Shilov catalyst. Center: A potential analogous $\text{Ir}^{\text{III}}/\text{Ir}^{\text{V}}$ cycle. Right: A potential analogous $\text{Rh}^{\text{I}}/\text{Rh}^{\text{III}}$ cycle.

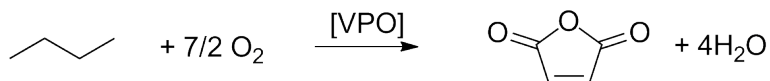
Chapter 2 focuses on bis(phenolate)pyridineiridium(III) ((ONO)Ir) complexes as an Ir analogue to the Shilov catalyst. Iridium as an alkane oxidation catalyst has been a popular choice; many

(primarily low-valent) Ir complexes have been reported to show good activity for C–H activation [7], and examples of oxidative functionalization with Ir systems are known as well [8]. Interconversions between Ir^{III} and Ir^V might be important in this chemistry, by analogy to the Shilov system, which involves Pt^{II} and Pt^{IV}. In Chapter 2, the experimental synthesis and characterization of a multitude of ((ONO)Ir) complexes in the +III and +IV oxidation state are described. In particular, the complex (ONO)Ir(PPh₃)₂Me has been found to undergo oxidation with iodine to release MeI, analogous to the Shilov system’s production of MeCl. Furthermore, (ONO)Ir(PPh₃)₂Me has been found to undergo an unusual C–H activation route with benzene that initially proceeds by intramolecular C–H activation, followed by intermolecular C–H activation.

Chapter 3 focuses on rhodium due to its well-documented nature as an effective C–H activating metal [9] and whose lower electronegativity may allow it to avoid poisoning by coordinating media. In this chapter, a computational screening of a variety of ligands was undertaken in order to find a Rh–ligand complex with the predicted optimal combination of low methane activation energy, low methyl group functionalization energy, and overoxidation protection of the MeX product. Our best results were the Rh^{III} bis(*N*-pentafluorophenyl)pentafluorobenzylamidinate (Rh^{III}(NN^F)) complex and the Rh^{III} bis(quinolinyl)benzene (Rh^{III}(bisq)) complex. In addition, we also report a correlation between Rh–Me bond energies and methane activation barriers that would allow us to easily predict the suitability of new complexes for methane activation.

1.2 Investigation and applications of the Reduction-Coupled Oxo Activation (ROA) mechanistic motif towards alkane upgrading.

Vanadium phosphorus oxide (VPO) is an inorganic complex that catalyzes the oxidation of *n*-butane to maleic anhydride with a surprisingly high selectivity of 60–70% [10] (Scheme 1.2). Although the overall yield is only *ca.* 50%, its ease of synthesis, use of common elements, and selectivity have allowed this catalyst to be commercialized, producing *ca.* 500 kilotons of maleic anhydride annually [11].

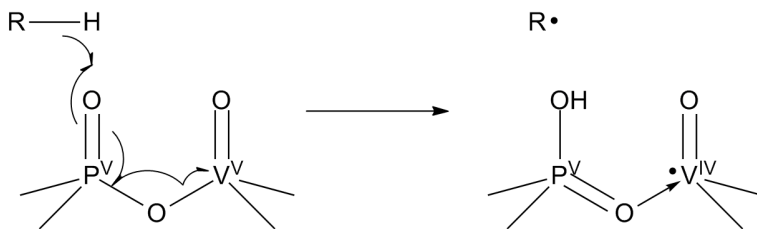


Scheme 1.2. The oxidation of *n*-butane to maleic anhydride using vanadium phosphorus oxide as a catalyst.

Surprisingly, the mechanism has been shown to initiate with C–H activation by a P=O moiety [12]. Whereas the many vanadium oxos and peroxos investigated bound with hydrogen with a

maximum energy of only 70.0 kcal/mol, too low for initial C–H activation of *n*-butane to occur, the phosphorus oxo has a much larger bond strength with hydrogen, at 84.3 kcal/mol. This implies a first step that is endothermic by only 5.0 kcal/mol, with an activation energy later calculated to be 13.6 kcal/mol, which is within the experimental range. The stability of the resulting mono-hydrogenated species was attributed to the fact that spin density appears to be localized on the neighboring vanadium atoms (Figure 1.1).

Figure 1.1. C–H activation by a phosphorus oxo leads to a one electron reduction on the neighboring vanadium. Hence the oxidation state of the phosphorus atom does not change.

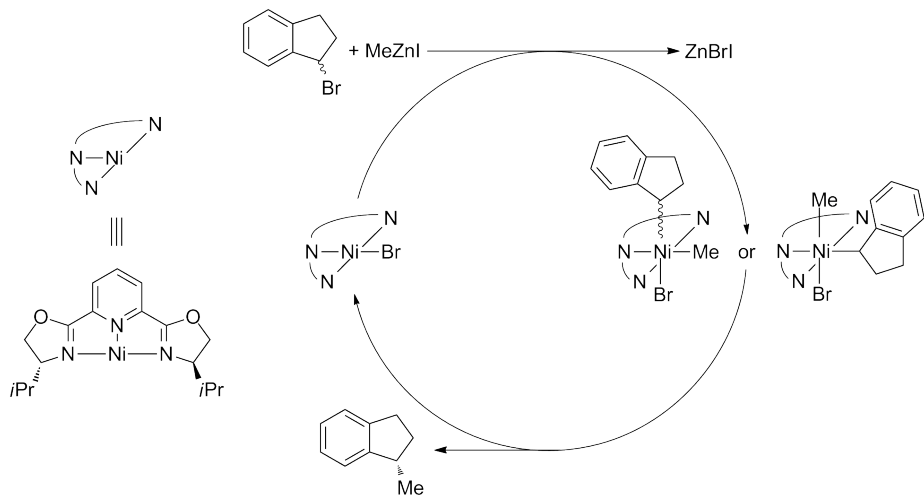


Chapter 4 focuses on deeper investigations into the ROA mechanistic motif. Specifically, questions such as the generalizability of the mechanism to other metal–main group pairs, as well as the applications of the ROA motif to homogeneous catalysts, are addressed. We have designed the homogeneous complex κ -P bis(2-phenoxy)phosphinite vanadium ((OPO)V) to be a catalyst that may activate propane using the ROA mechanistic motif. We then continued to follow the reaction forward, tracing pathways for the catalytic oxidation of propane in aqueous solution using O_2 as the terminal oxidant. We found that the ((OPO)V) system has the potential to be a viable catalyst in acidic aqueous solution, converting propane to either propylene or isopropanol.

1.3 Other projects

Chapter 5 is a computational mechanistic study of the 2,6-bis(4-isopropyl-2-oxazolin-2-yl)pyridine nickel ($Ni((iPr)-pybox)$) system, a Negishi C–C coupling catalyst. In our computational work, we investigated the coupling of 1-bromoindane with methylzinc iodide catalyzed by the $Ni((S,S-iPr)-pybox)$ system to form 1-methylindane. The chiral diastereomers of this catalyst are most notable for their stereoconvergence: Using $Ni((S,S-iPr)-pybox)$ as a catalyst, both enantiomers of racemic 1-bromoindane will couple with methylzinc iodide to form (*S*)-1-methylindane with 90% enantiomeric excess [?]. We confirm that the mechanism proceeds through a Ni^I-Ni^{III} couple, in contrast to the classic Ni^0-Ni^{II} cycle that Negishi catalysts are typically assumed to undergo [?] (Scheme 1.3).

Appendix A is an experimental and computational study of the (L) $Rh^I(COE)(TFA)$ complexes in which L is DAB^F or BOZO (DAB^F = *N,N*-bis(pentafluorophenyl)-2,3-dimethyl-1,4-diaza-1,3-butadiene, COE = cyclooctene, TFA = trifluoroacetate, BOZO = bis(2-oxazolin-2-yl)). These com-



Scheme 1.3. The generalized mechanism of the $\text{Ni}((i\text{Pr})\text{-pybox})$ Negishi coupling catalyst as it proceeds through a $\text{Ni}^{\text{I}}\text{-Ni}^{\text{III}}$ cycle. The overall equation is $\text{ind-Br} + \text{MeZnI} \longrightarrow \text{ind-Me} + \text{ZnBrI}$.

plexes have been shown to catalyze the H/D exchange of benzene in trifluoroacetic acid. Computationally, the mechanism was found to occur by the reversible oxidative addition and reductive elimination of benzene to and from the $(\text{L})\text{Rh}^{\text{I}}(\text{TFAH})(\text{TFA})$ species.

Appendix B is a comparison of various DFT and electron-correlation methods for calculating the group 10 transition metals Ni, Pd, and Pt. These elements are notable in that, despite being in the same periodic group, they each have a different electronic configuration (d^8s^2 , d^{10} , and d^9s^1 , respectively). The accuracy of DFT and electron-correlation methods in reproducing the transition energies between the three configurations for the three elements is an important consideration that has deeper implications in the reactivity of more complex systems including these elements.

1.4 References

- [1] Cheng, W-H.; Kung, H. H. *Methanol Production and Use (Chemical Industries vol. 57)*, **1994**.
- [2] IPCC Fourth Assessment Report, Working Group 1, Chapter 2.
- [3] (a) Labinger, J. A.; Bercaw, J. E. *Nature* **2002**, *417*, 507–514;
(b) Crabtree, R. H. *J. Chem. Soc., Dalton Trans.* **2001**, 2437–2450;
(c) Labinger, J. A. *Fuel Proc. Technol.* **1995**, *42*, 325–338;
(d) Labinger, J. A. *J. Mol. Catal. A: Chem.* **2004**, *220*, 27–35.
- [4] (a) Fekl, U.; Goldberg, K. I. *Adv. Inorg. Chem.* **2003**, *54*, 259–320;
(b) Lersch, M.; Tilset, M. *Chem. Rev.* **2005**, *105*, 2471–2526.
- [5] (a) Goldshlegger, N. F.; Tyabin, M. B.; Shilov, A. E.; Shtainman, A. A. *Zh. Fiz. Khim.* **1969**, *43*, 2174–2175;
(b) Goldshlegger, N. F.; Eskova, V. V.; Shilov, A. E.; Shtainman, A. A. *Zh. Fiz. Khim.* **1972**, *46*, 1353–1354;
(c) Shilov, A. E.; Shul’pin, G. B. *Activation and Catalytic Reactions of Saturated Hydrocarbons in the Presence of Metal Complexes*; Kluwer Academic Publishers: Dordrecht, **2000**; pp. 259–317.
- [6] Periana, R. A.; Taube, D. J.; Evitt, E. R.; Loffler, D. G.; Wentzcek, P. R.; Voss, G.; Masuda, T. *Science* **1993**, *259*, 340–343.
- [7] Arndtsen, B. A.; Bergman, R. G.; Mobley, T. A.; Peterson, T. H. *Acc. Chem. Res.* **1995**, *28*, 154–162.
- [8] (a) Wong-Foy, A. G.; Bhalla, G.; Liu, X. Y.; Periana, R. A. *J. Am. Chem. Soc.* **2003**, *125*, 14292–14293;

(b) Oxgaard, J.; Muller, R. P.; Goddard, W. A.; Periana, R. A. *J. Am. Chem. Soc.* **2004**, *126*, 352–363;

(c) Bhalla, G.; Liu, X. Y.; Oxgaard, J.; Goddard, W. A.; Periana, R. A. *J. Am. Chem. Soc.* **2005**, *127*, 11372–11389;

(d) Tenn, W. J.; Young, K. J. H.; Bhalla, G.; Oxgaard, J.; Goddard, W. A.; Periana, R. A. *J. Am. Chem. Soc.* **2005**, *127*, 14172–14173;

(e) Bhalla, G.; Periana, R. A. *Angew. Chem., Int. Ed.* **2005**, *44*, 1540–1543;

(f) Young, K. J. H.; Mironov, O. A; Periana, R. A. *Organometallics* **2007**, *26*, 2137–2140;

(g) Young, K. J. H.; Oxgaard, J.; Ess, D. H.; Meier, S. K.; Stewart, T.; Goddard, W. A.; Periana, R. A. *Chem. Commun.* **2009**, 3270–3272.

[9] (a) Arndtsen, B. A.; Bergman, R. G.; Mobley, T. A.; Peterson, T. H. *Acc. Chem. Res.* **1995**, *28*, 154–162;

(b) Hanson, S. K.; Heinekey, D. M.; Goldberg, K. I. *Organometallics* **2008**, *27*, 1454–1463;

(c) Evans, M. E.; Jones, W. D. *Organometallics* **2011**, *30*, 3371–3377;

(d) Zakzeski, J. J.; Bell, A. T. *J. Mol. Cat. A: Chem.* **2007**, *276*, 8–16;

(e) Zhang, X. X.; Wayland, B. B. *J. Am. Chem. Soc.* **1994**, *116*, 7897–7898;

(f) Tenn, W. J. III; Conley, B. L.; Bischof, S. M.; Periana, R. A. *J. Organomet. Chem.* **2011**, *696*, 551–558;

(g) Rhinehart, J. L.; Manbeck, K. A.; Buzak, S. K.; Lippa, G. M.; Brennessel, W. W.; Goldberg, K. I.; Jones, W. D. *Organometallics* **2012**, *31*, 1943–1952;

(h) Li, L.; Brennessel, W. W.; Jones, W. D. *Organometallics* **2009**, *28*, 3492–3500;

(i) Kloek, S. M.; Heinekey, D. M.; Goldberg, K. I. *Angew. Chem. Int. Ed.* **2007**, *46*, 4736–4738.

[10] Centi, G.; Trifiro, F.; Ebner, J. R.; Franchetti, V. M. *Chem. Rev.* **1988**, *88*, 55–80.

[11] Hodnett, B. K. *Heterogeneous Catalytic Oxidation*. Wiley: New York, **2000**.

[12] Cheng, M.-J. and Goddard, W. A. *J. Am. Chem. Soc.* **2013**, *135*, 4600–4603.